Available online at www.sciencedirect.com
ScienceDirect
Image and Vision Computing 25 (2007) 1785–1801
image AND vision COMPUTING
www.elsevier.com/locate/imavis

Automated visual inspection of ripple defects using wavelet characteristic based multivariate statistical approach

Hong-Dar Lin *

Department of Industrial Engineering and Management, Chaoyang University of Technology, 168 Jifong E. Road, Wufong Township, Taichung County 41349, Taiwan, ROC

Received 13 June 2005; received in revised form 1 January 2007; accepted 2 February 2007

Abstract

This paper presents a wavelet characteristic based approach for the automated visual inspection of ripple defects in the surface barrier layer (SBL) chips of ceramic capacitors. Difficulties exist in automatically inspecting ripple defects because of their semi-opaque and unstructured appearances, the gradual changes of their intensity levels, and the low intensity contrast between their surfaces and the rough exterior of a SBL chip. To overcome these difficulties, we first utilize wavelet transform to decompose an image and use wavelet characteristics as texture features to describe surface texture properties. Then, we apply multivariate statistics of Hotelling T^2, Mahalanobis distance D^2, and Chi-square X^2, respectively, to integrate the multiple texture features and judge the existence of defects. Finally, we compare the defect detection performance of the three wavelet-based multivariate statistical models. Experimental results show that the proposed approach (Hotelling T^2) achieves a 93.75% probability of accurately detecting the existence of ripple defects and an approximate 90% probability of correctly segmenting their regions.

Keywords: Detection of ripple defects; Machine vision; Hotelling T^2 multivariate statistics; Wavelet characteristics

1. Introduction

This research aims to construct a machine vision system for inspecting ripple defects in surface barrier layer (SBL) chips, one kind of work in process of ceramics capacitors. Ripple defects, commonly found in the randomly textured surfaces of SBL chips, are formed by the steam generated during the production process. The defects affect the appearances of SBL chips as well as the electronic properties of the products. Difficulties exist in automatically inspecting ripple defects because: (1) ripple defects are semi-opaque; (2) ripple defects have unstructured shapes; (3) the intensity levels of a ripple defect change gradually; (4) the surface of a SBL chip is rough and its intensity levels are close to those of its ripple defects (low contrast). As seen in Fig. 1, the three images contain ripple defects of different shapes and the intensity levels of the defects change gradually. Nevertheless, difficulties also exist in detecting ripple defects by human eyes because inspectors are very likely to make erroneous judgments due to personal subjectivity or eye fatigues. Seeing the great need and usefulness of an automatic inspection system, we apply wavelet transform and multivariate statistical models to construct a machine vision system for detection of ripple defects.

Texture analysis, an important step in the image processing procedure, can be applied in various areas, such as diagnosing pathological changes of tumor cells in medical images, detecting surface defects of industrial parts, and remote sensing. The main tasks of texture analysis involve classification, segmentation, and synthesis [1]. Textures are generally classified into two categories: structural and statistical [2]. Structural textures consist of repetitions of some basic texture primitives, such as lines, arcs or circles, with a definite displacement rule. They have regular and homogeneous properties and arise commonly in textile

* Tel.: +886 4 2332 3000x4258; fax: +886 4 2374 2327.
E-mail address: hdlin@cyut.edu.tw

0262-8856/$ - see front matter © 2007 Elsevier B.V. All rights reserved.
doi:10.1016/j.imavis.2007.02.002

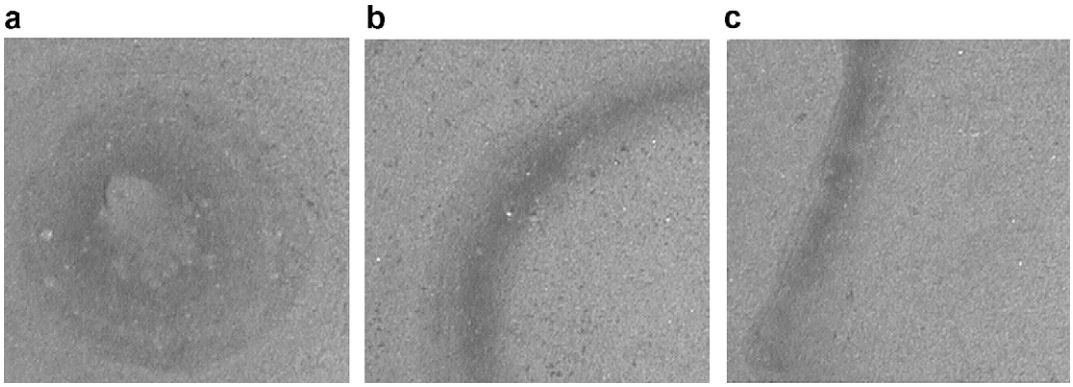

Fig. 1. Ripple defects of different shapes.

fabrics and machined surfaces. Numerous methods have been designed to solve the structural defect inspection tasks in textile fabrics [3–5]. On the other hand, statistical textures, also called random textures, cannot be described by primitives and displacement rules. They arise randomly in object surfaces, such as sandpapers, leathers, and cast surfaces. Surface defects locally break the homogeneity of a texture pattern. In general inspection of random textures [6–10], most researchers do not consider how the gradual changes of image properties impact the defect inspection results, even if some defects do have gradual changes of image properties. In this research, we present a wavelet-based multivariate statistical approach for inspecting semi-opaque, unstructured and low contrast ripple defects that have gradually changing intensity levels at their edges.

Automatic techniques for the visual inspection of textured surfaces usually compute a set of textural features in a sliding window and search for significant local deviations in the feature values. Generally, there are two types of texture analysis techniques: spatial domain and frequency domain. The traditional method for texture analysis in the spatial domain is to extract various features from a gray level co-occurrence matrix. This approach is based on the use of second-order statistics of the grayscale image histogram. Siew et al. [11] use two-order gray level statistics to build up probability density functions of intensity changes, and develop co-occurrence matrices for carpet wear assessment. Also, Venkat Ramana and Ramamoorthy [12] present the co-occurrence matrix based statistical methods to compare the texture features of machined surfaces.

Fourier transform, Gabor transform and wavelet transform are common texture analysis techniques used in the frequency domain [1]. Fourier-based methods characterize the spatial frequency distribution of textured images, but they do not consider the information in the spatial domain and may ignore local deviations [10]. Chan and Pang [13] introduce the central spatial frequency spectrum approach to classify four defects of textile fabrics based on seven characteristic parameters of the Fourier spectrum. Gabor-filter-based approaches have been successfully applied for texture analysis [9,10], but the design of optimal Gabor filters is a complicated task and these methods are computationally expensive since the 2-D convolution must be conducted in a sliding window throughout the entire image. In addition, Gabor filters require proper tuning of filter parameters at different scales [14]. Kumar and Pang [15] propose supervised and unsupervised defect detection approaches for automated inspection of textile fabrics using Gabor wavelet features.

Wavelet transform provides a convenient way to obtain a multiresolution representation, from which texture features are easily extracted. It has been a popular alternative for the extraction of textural features. Since images in different scales and frequencies have inherent characteristics for the appearance of a texture, the multi-resolution, multi-channel modeling capability of wavelets is well suited for texture analysis [16]. The use of the wavelet transform for texture analysis was pioneered by Mallat [17]. Textureal features extracted from wavelet-decomposed images are widely used for texture classification, segmentation, object recognition, and defect detection [18–21]. Latif-Amet et al. [22] propose a sub-band domain co-occurrence matrix method for texture defect detection. Their approach is performed first by decomposing the gray level images into sub-bands, then by partitioning the textured image into non-overlapping sub-windows and extracting the co-occurrence features and finally by classifying the defective sub-windows with statistical classifier. Huang and Aviyente [23] develop an algorithm to choose independent subbands to form a sparse representation of texture images for classification. Cui et al. [24] propose an effective method for rotation and scaling invariant texture classification based on wavelet analysis in the Radon domain.

Color and texture are two of the most important properties in analyzing complicated material surfaces. Color can provide powerful information for texture analysis, but traditional texture analysis techniques are inappropriate for colored texture images because they ignore chromatic information. More sophisticated color imaging methods have been developed for color texture classification and defect detection [25,26]. Wouwer et al. [27] introduce wavelet energy-correlation signatures extracted from features of wavelet-decomposed images for color texture characteriza-

tion. The extracted features combine image color and texture information for adequately describing the concept of color texture.

The wavelet transform methods aforementioned for texture analysis are generally based on extraction of textural features in different scales and subbands. Some developed methods do not rely on textural features to detect local anomalies. Tsai and Hsiao [16] propose an image restoration scheme using the multiresolution wavelet transforms for the inspection of local defects embedded in homogeneous textured surfaces. By properly selecting the smooth subimage or the combination of detail subimages in different decomposition levels for backward wavelet transform, regular, repetitive texture patterns can be removed and only local anomalies are enhanced in the reconstructed image. This method results in considerable computational savings. Nagan et al. [28] develop the wavelet preprocessed golden image subtraction (WGIS) method for defect detection on respective patterned texture. The WGIS method achieves a smoothing effect on the incoming histogram equalized image and then applies a convolution filter on approximated subimages decomposed by the Haar wavelet transform to detect defects on the dot-patterned fabric. These wavelet-based techniques perform well in texture analysis. But, most of the existing wavelet-based texture analysis methods do not detect defects with the properties of ripple defects [3–9,13–16,22,26,28].

Our work has been motivated by the need of an efficient and effective technique that detects and locates ripple defects in colored texture surfaces. In this study, we are considering an automatic surface inspection problem, in which defect-free samples of the textures of interest are given a priori. The surface defect inspection method of this research, though also applied in the frequency domain, is different from existing techniques. We use the one-level Haar wavelet transform to conduct colored image pre-processing for extraction of image features, because the merits of wavelet transform include local image processing, simple calculations, high speed processing and multiple image information. Then, we apply three different multivariate statistics, T^2, X^2, and D^2, that integrate multiple quality characteristics to synthesize multiple image features. After image features are combined, the statistic values are used to judge the existence of defects. This wavelet-based multivariate statistical approach is ideally suited for describing locally gradual changes in a homogeneous textured image.

The main contribution of this paper is in applying Hotelling T^2 statistic to build a new wavelet-based multivariate statistical model of automated visual inspection system for ripple defect detection in random textures. Specially, Hotelling T^2 test, a multivariate statistical process control (SPC) technique is used to analyze surface inspection of activities in machine vision system and detect ripple defects in the random surface. The effectiveness of the proposed approach is demonstrated by experiments on real chip images.

In multivariate statistical analysis, the Hotelling T^2 control chart, the most renowned multivariate process monitoring and control procedure, was proposed by Hotelling [29] for monitoring the mean vector of a process. The purpose of the Hotelling control chart is to control a process with multiple quality characteristics, to which traditional Shewhart control charts cannot be applied. Many researchers study the control limits of the multivariate control chart. Alt [30] proposes the multivariate control limits for estimated mean and variance when the sample size is less than 25. Jolayemi [31] presents an effective calculation formula for determination of sample sizes. Mason and Young [32], and Mason et al. [33] develop a method that increases the sensitivity of the T^2 statistics of the multivariate process, and apply it to a batch process. As complexities in production techniques increase, more and more multivariate control charts are applied to monitor industrial processes [34–36].

The remainder of the paper is organized as follows: Section 2 describes three multivariate statistical analysis techniques based on Hotelling T^2, Mahalanobis distance D^2, and Chi-square X^2, respectively. Section 3 presents the developed wavelet characteristic based multivariate statistical approach. Section 4 demonstrates the experiments on the performance evaluation of the proposed methods and discusses the experimental results and comparisons. Finally, the paper concludes with suggestions for future work.

2. Multivariate statistical analysis

In this section, we first describe Hotelling's T^2 test, Mahalanobis distance D^2, and Chi-square X^2 test. Then, we compare these three techniques, and discuss their differences from statistical viewpoint.

2.1. Hotelling T^2 control chart

Lowry and Montgomery [37], and Montgomery [38] compare the procedures and functions of multivariate control charts in detail. It is assumed that the joint probability distribution of the p quality characteristics is the p-variate normal distribution. The procedure requires computing the sample mean for each of the p quality characteristics from a sample of size n. The set of quality characteristic means is represented by the $p \times 1$ vector: $\bar{x}' = [\bar{x}_1, \bar{x}_2, \ldots, \bar{x}_p]$. The test statistic plotted on the Hotelling T^2 control chart for each sample is

$$T^2 = n(\bar{x} - \boldsymbol{\mu})^{\mathrm{T}} \boldsymbol{\Sigma}^{-1} (\bar{x} - \boldsymbol{\mu}) \tag{1}$$

where $\boldsymbol{\mu}^{\mathrm{T}} = [\mu_1, \mu_2, \ldots, \mu_p]$ is the vector of in-control means for each quality characteristic and $\boldsymbol{\Sigma}$ is the covariance matrix. The two vectors of in-control means $\boldsymbol{\mu}$ and covariance matrix $\boldsymbol{\Sigma}$ are both unknown in the Hotelling T^2 control chart. Therefore, it is usually necessary to estimate $\boldsymbol{\mu}$ and $\boldsymbol{\Sigma}$ from the analysis of the preliminary sample of size n when the process is assumed to be in control. Supposing

m of such samples are available, the sample means and variances are calculated from each sample as usual; that is,

$$\bar{x}_{jk} = \frac{1}{n}\sum_{i=1}^{n} x_{ijk}, \quad j = 1,2,3,\ldots,p,\ k = 1,2,3,\ldots,m \tag{2}$$

$$s_{jk}^2 = \frac{1}{n-1}\sum_{i=1}^{n}(x_{ijk} - \bar{x}_{jk})^2 \quad j = 1,2,3,\ldots,p,\ k = 1,2,3,\ldots,m \tag{3}$$

where x_{ijk} is the ith observation on the jth quality characteristic in the kth sample. The covariance between quality characteristic j and quality characteristic h in the kth sample is:

$$s_{jhk} = \frac{1}{n-1}\sum_{i=1}^{n}(x_{ijk} - \bar{x}_{jk})(x_{ihk} - \bar{x}_{hk}) \quad k = 1,2,3,\ldots,m,\ j \neq h \tag{4}$$

The statistics $\bar{x}_{jk}$, s_{jk}^2, and s_{jhk} are then averaged over all m samples to obtain:

$$\bar{\bar{x}}_j = \frac{1}{m}\sum_{k=1}^{m}\bar{x}_{jk} \quad j = 1,2,3,\ldots,p$$

$$\bar{s}_j^2 = \frac{1}{m}\sum_{k=1}^{m}s_{jk}^2 \quad j = 1,2,3,\ldots,p \tag{5}$$

$$\bar{s}_{jh} = \frac{1}{m}\sum_{k=1}^{m}s_{jhk} \quad j \neq h$$

The $\{\bar{\bar{x}}_j\}$ are the elements of the vector $\bar{\bar{X}}$, and the $p \times p$ average of sample covariance matrices $\mathbf{S}$ is represented as:

$$\mathbf{S} = \begin{bmatrix} \bar{s}_1^2 & \bar{s}_{12} & \cdots & \bar{s}_{1p} \\ & \bar{s}_2^2 & \cdots & \bar{s}_{2p} \\ & & \ddots & \vdots \\ & & & \bar{s}_p^2 \end{bmatrix}. \tag{6}$$

The average of the sample covariance matrices $\mathbf{S}$ is an unbiased estimate of $\boldsymbol{\Sigma}$ when the process is in control. If we replace $\boldsymbol{\mu}$ with $\bar{\bar{X}}$, and $\boldsymbol{\Sigma}$ with $\mathbf{S}$; the test statistic becomes:

$$T^2 = n(\bar{X} - \bar{\bar{X}})^{\mathrm{T}}\mathbf{S}^{-1}(\bar{X} - \bar{\bar{X}}). \tag{7}$$

When $\boldsymbol{\mu}$ and $\boldsymbol{\Sigma}$ are estimated from a number of preliminary samples, the control limits are as follows:

$$\mathrm{UCL} = \frac{p(m-1)(n-1)}{mn - m - p + 1}F_{\theta,p,(mn-m-p+1)}; \quad \mathrm{LCL} = 0. \tag{8}$$

If the T^2 value is greater than the UCL for a given level of significance θ, then we reject the null hypothesis that the process is in control (normal) and thus signal that the process is out of control (anomalous).

2.2. Mahalanobis distance

The Mahalanobis distance is a measure of the distance from an individual point to the centroid of a population multidimensional space based on the assumption of a multivariate normal distribution $N(\mu, \Sigma)$ for the population. Mahalanobis distance is expressed as follows:

$$D_i^2 = (\bar{x}_i - \mu)^{\mathrm{T}}\Sigma^{-1}(\bar{x}_i - \mu) \tag{9}$$

where $\bar{x}_i$ is a vector representing a set of means of quality characteristics from a sample of size n; μ is a vector representing the centroid of the population; and Σ is the variance–covariance matrix of the population. In practice, the estimated mean vector and variance–covariance matrix from sample sets of m are used to replace μ and Σ.

Different threshold rules are used in various applications of Mahalanobis distance [25,26]. Latif-Amet et al. [20] propose the threshold value D_{T}^2 determined by the following formula to identify defective regions:

$$D_{\mathrm{T}}^2 = D_{\mathrm{m}}^2 + \eta(D_{\mathrm{q}}^2 - D_{\mathrm{m}}^2) \tag{10}$$

D_{m}^2 and D_{q}^2 are, respectively, the sample median and the sample upper quartile of the order statistics D_i^2 obtained when distances are arranged in ascending order and η is a constant determined experimentally. If a D_i^2 value exceeds a threshold value D_{T}^2 as defective, else identify it as non-defective.

2.3. Chi-square X^2 test

Ye et al. [39] developed the X^2 test, a multivariate statistical technique based on the chi-squared distance test. The X^2 test performs well in detecting intrusions into information systems. The X^2 test and its performance are used for evaluating the performance of the T^2 test in this research. If we have p variables to measure and X_j denotes the observation of the jth ($1 \leqq j \leqq p$) variable at a particular time, the X^2 test statistic is given by the equation:

$$X^2 = \sum_{j=1}^{p}\frac{(X_j - \overline{X_j})^2}{\overline{X_j}} \tag{11}$$

This test statistic measures the distance of a data point from the center of a data population. Hence, it is called the chi-square distance test. Using a sample of X^2 values, the mean and standard deviation of the X^2 population can be estimated from the sample mean $\overline{X^2}$ and the sample standard deviation S_{X^2}. The in-control limits to detect out-of-control anomalies are usually set to 3-sigma control limits, as determined by $[\overline{X^2} - 3S_{X^2}, \overline{X^2} + 3S_{X^2}]$. Since we are interested in detecting significantly large X^2 values, we need to set only the upper control limit to $\overline{X^2} + 3S_{X^2}$ as a signal threshold. That is, if the X^2 for an observation is greater than $\overline{X^2} + 3S_{X^2}$, we signal an anomaly.

2.4. Comparison of the T^2 test, X^2 test, and D^2 test

Each of the T^2, D^2, and X^2 statistics measures the distance of an observation from the multivariate mean vector of a population. The T^2 and D^2 test statistics use the statistical distance that incorporates the multivariate variance–

covariance matrix [40], whereas X^2 test statistic uses the chi-squared distance. The chi-squared distance, similar to a Euclidean distance, uses the average value on each variable to scale the Euclidean distance on that variable.

Anomalies involving multiple variables can be caused by shifts from the means of these variables (mean shifts), departures from variable relationships (correlation changes), or combinations of mean shifts and correlation changes. In contrast to the T^2 and D^2 statistics, the X^2 statistic does not account for the correlated structure of the multiple variables. Hence, the T^2 and D^2 tests detect both mean shifts and correlation changes, whereas the X^2 test detects only the mean shift on one or more of the multiple variables.

The differences between T^2 test and D^2 test are in whether the influence of sample size on hypothesis testing is considered and whether a consistent decision interval is provided. The D^2 does not take into account how sample size impacts hypothesis testing. In some situations, when the sample size is large and though the statistic D^2 is small, the hypothesis testing task may end up in rejecting the null hypothesis. The probability of making erroneous judgement is increased for the lack of considering the impact of sample size. In addition, the D^2 does not provide a consistent decision interval for different applications have different threshold formulas. Hair et al. [41] indicate Mahalanobis distance is limited in the purpose of identifying outliers because threshold values depend on a number of factors, and a rule of thumb threshold value is not possible. Nevertheless, the T^2 statistic not only takes into account the D^2 distance and sample size but also provides the same decision interval.

3. Proposed method

This research utilizes the concept of the multivariate statistical approach, commonly used in monitoring the mean vector of a multivariate process, to inspect ripple defects embedded in homogeneous texture surface. By means of wavelet transform decomposition, the proposed method first uses wavelet characteristics such as texture features to describe surface texture properties. Then, the multivariate statistics of Hotelling T^2 control chart are applied to integrate the multiple texture features and judge the existence of ripple defects in the image.

3.1. Wavelet decomposition

Wavelet transform decomposes the function V_j in terms of the wavelet bases $V_{j-1} \oplus W_{j-1}$. That is, the wavelet analysis can deal with the decomposition and synthesis of V_j and V_{j+1} in two-level scaling space. Decomposition conducts a forward wavelet analysis to decompose the base V_{j+1} into bases V_j and W_j. Synthesis performs a backward wavelet analysis to reconstruct V_j and W_j into V_{j+1} [17].

The Haar wavelet transform is one of the simplest and basic transformations. Its base transform in the multiple-level scaling space can be implemented as:

$$v_{j,k} = \frac{v_{j+1,2k} + v_{j+1,2k+1}}{2}; \quad w_{j,k} = \frac{v_{j+1,2k} - v_{j+1,2k+1}}{2}. \tag{12}$$

In this research, we apply a standard decomposition that covers wavelet row and column transfers to do the wavelet transform of a two-dimensional image. The Haar transform can be computed stepwise by the mean value and half of the differences of the tristimulus values of two contiguous pixels. We perform the 2-D wavelet transform by applying 1-D wavelet transform first on rows and then on columns. Based on the transfer concept of the one-dimensional space, the Haar wavelet transform can process a two-dimensional image of $(S \times T)$ pixels in the following way:

Row transfer :

$$\begin{cases} f_R(i,j) = \left[\frac{f(i,2j)+f(i,2j+1)}{2}\right], \\ f_R\left(i, j+\left[\frac{T}{2}\right]\right) = \left[\frac{f(i,2j)-f(i,2j+1)}{2}\right], \\ \text{where } 0 \leqslant i \leqslant (S-1), 0 \leqslant j \leqslant \left[\frac{T}{2}\right]-1, [\,] \text{ is Gauss symbol.} \end{cases} \tag{13}$$

Column transfer :

$$\begin{cases} f_C(i,j) = \left[\frac{f_R(2i,j)+f_R(2i+1,j)}{2}\right], \\ f_C\left(i+\left[\frac{S}{2}\right], j\right) = \left[\frac{f_R(2i,j)-f_R(2i+1,j)}{2}\right], \\ \text{where } 0 \leqslant i \leqslant \left[\frac{S}{2}\right]-1, 0 \leqslant j \leqslant (T-1), [\,] \text{ is Gauss symbol.} \end{cases} \tag{14}$$

In the above expressions, $f(i,j)$ represents an original image, $f_R(i,j)$ the row transfer function of $f(i,j)$, and $f_C(i,j)$ the column transfer function of $f_R(i,j)$. As $f_C(i,j)$ is also the outcome of wavelet decomposition of $f(i,j)$, we can define the outcomes of a wavelet transform as:

$$\begin{cases} A_1(i,j) = f_C(i,j), \\ D_1(i,j) = f_C\left(i, j+\left[\frac{T}{2}\right]\right), \\ D_2(i,j) = f_C\left(i+\left[\frac{S}{2}\right], j\right), \\ D_3(i,j) = f_C\left(i+\left[\frac{S}{2}\right], j+\left[\frac{T}{2}\right]\right), \\ \text{where } 0 \leqslant i \leqslant \left[\frac{S}{2}\right]-1, \quad 0 \leqslant j \leqslant \left[\frac{T}{2}\right]-1, \end{cases} \tag{15}$$

$A_1(i,j)$ is a smooth subimage and represents the coarse approximation of the image $f(i,j)$. $D_1(i,j), D_2(i,j)$, and $D_3(i,j)$ are detail subimages and represent the horizontal, vertical and diagonal directions of the image $f(i,j)$, respectively.

3.2. Wavelet characteristics

Selecting the right combination of texture features that appropriately describes the texture properties is crucial for obtaining the best performance of texture analysis techniques. For example, the combination of scale, frequency and orientation features contributes to the effective performance of Gabor transform [9,10]. Nevertheless, since this research deals with unstructured ripple defects in random textures, difficulties exist in extracting suitable texture features to characterize texture properties of an image in the spatial domain. Thus, we use wavelet characteristics from

decomposing an image by wavelet transform as texture features to describe surface textured properties in this research. An original image is decomposed into four subimages: one low-pass filtering subimage (approximation image) and three high-pass filtering subimages (detail images).

An original image of $(S \times T)$ pixels is decomposed by wavelet transform into a set of equal-size subimages: one approximated subimage (A_1) and three detail subimages $(D_1, D_2, \text{and } D_3)$. Each subimage has a size of $(\frac{S}{2} \times \frac{T}{2})$ pixels. Since the three detail subimages represent different image features, information fusion methods can be used to integrate the multiple detail subimages into synthetic feature values. The purpose of image fusion is to enhance the original image features. We define the wavelet characteristics of an image, its approximated feature (A) and detail feature (D) as follows:

$$A = \frac{\sum_{i=0}^{\frac{S}{2}-1}\sum_{j=0}^{\frac{T}{2}-1}[A_1(i,j)]}{\left(\frac{S}{2} \times \frac{T}{2}\right)},$$
$$D = \frac{\sum_{i=0}^{\frac{S}{2}-1}\sum_{j=0}^{\frac{T}{2}-1}[w_1 D_1(i,j) + w_2 D_2(i,j) + w_3 D_3(i,j)]}{\left(\frac{S}{2} \times \frac{T}{2}\right)}, \quad (16)$$
$$\text{and } w_1 + w_2 + w_3 = 1,$$

where equal weighted values $(w_1 = w_2 = w_3)$ are used in the research for treating the three detail subimages as equally important.

3.3. Wavelet characteristic based multivariate T^2 model

The proposed multivariate statistical model decomposes an image of $(M \times N)$ pixels into a set of equal-size subimages, which are called units of multivariate processing. Supposing each of the subimages has $(m \times n)$ pixels, then the original image has $g \times h$ (i.e. $\frac{M}{m} \times \frac{N}{n}$) multivariate processing units. Each of the multivariate processing units can be further decomposed into $a \times b$ wavelet processing units. For each wavelet processing unit, we can apply wavelet transform to the region of $(\frac{m}{a} \times \frac{n}{b})$ pixels to obtain two wavelet characteristics A and D. The multivariate statistic (e.g. T^2, D^2, or X^2) integrates the multiple wavelet characteristics into a statistic value for each multivariate processing unit. This statistic value can be regarded as a distance value of a multivariate processing unit. The larger the statistic value, the larger the difference between the region and the normal area, and the more this region can be judged as a defect region.

Any pixel of a RGB colour image can be decomposed into three components: R, G, and B. In the proposed multivariate statistical model, we use the same processing procedures to obtain image features for each of the three components. Fig. 2 demonstrates how the multivariate T^2 statistic model works. Assuming a multivariate processing unit has 4×4 (i.e. $m \times n$) pixels and a wavelet processing unit has 2×2 (i.e. $a \times b$) pixels, then one multivariate processing unit will have 2×2 (i.e. $\frac{m}{a} \times \frac{n}{b}$) wavelet processing units. By applying wavelet transform to a wavelet processing unit of 2×2 pixels, we can decompose the unit and extract one approximated (A) and three detail $(D_1, D_2, \text{and } D_3)$ wavelet characteristics. The three detail characteristics can be fused into a synthetic detail characteristic (D). Thus, an image of 256×256 pixels will have 64×64 (i.e. $g \times h$) sets of wavelet characteristics after a wavelet transform is implemented. Eqs. (5) and (6) calculate the mean value $(\overline{\overline{X}})$ and the covariance matrix (S) of the texture features of a normal image. By executing the same procedures to the testing images, we can get a mean matrix $(\overline{X})$ for each multivariate processing unit of 4×4 pixels. The $\overline{X}$ can be integrated to produce a T^2 value through T^2 statistic (Eq. (7)). Therefore, one image of 256×256 pixels can construct a T^2 distance diagram with 64×64 T^2 values.

An image can be divided into many multivariate processing units. Let a multivariate processing unit be $M(x,y)$ and an original image be $f(i,j)$. Fig. 3 presents the scopes of one multivariate processing unit and four wavelet processing units in the multivariate statistical model. Four wavelet processing units $C(x_a,y_b)$ can be defined in one multivariate processing unit $M(x,y)$, where a and b are integers and $(1 \leqq a, b \leqq 2)$. Thus, one $M(x,y)$ includes four

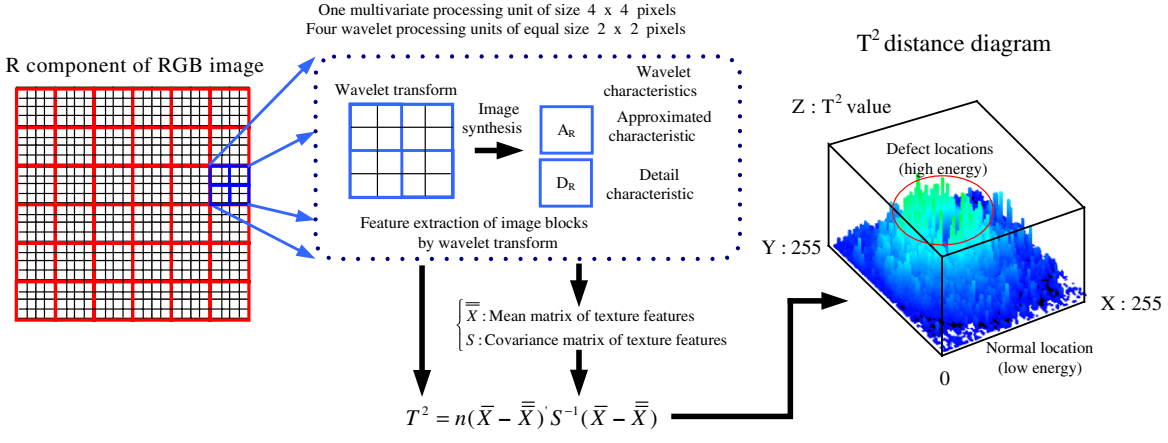

Fig. 2. The processes of the wavelet-based multivariate T^2 model.

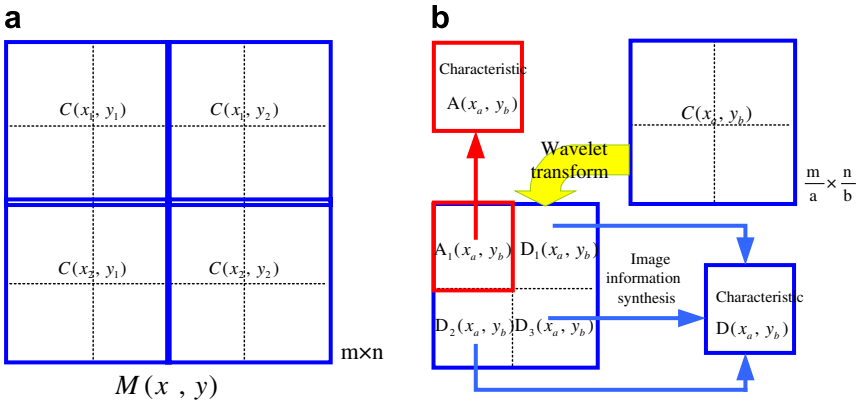

Fig. 3. Scope diagrams of a multivariate processing unit and wavelet processing units in the multivariate statistical model. (a) Multivariate processing unit $M(x,y)$. (b) Wavelet processing units $C(x_a,y_b)$.

$C(x_a,y_b)$ values, which are $C(x_1,y_1)$, $C(x_1,y_2)$, $C(x_2,y_1)$ and $C(x_2,y_2)$. One $C(x_a,y_b)$ can be decomposed by wavelet transform to obtain one approximated characteristic $A(x_a,y_b)$ and three detail characteristics $D_1(x_a,y_b)$, $D_2(x_a,y_b)$ and $D_3(x_a,y_b)$. The three detail characteristics are then fused into a synthetic detail characteristic $D(x_a,y_b)$.

The proposed approach can be extensively applied to multiple colour components. That is, $A_R(x,y)$ is the approximated characteristic and $D_R(x,y)$ is the detail characteristic for R component at (x,y). Similarly, $A_G(x,y)$ and $D_G(x,y)$ are for G component; and $A_B(x,y)$ and $D_B(x,y)$ are for B component. Therefore, we can adapt the multivariate T^2 statistic formulas in Eqs. (2)–(6) and present the multivariate process of the images in Eqs. (17)–(22).

$$\overline{X}_{M(x,y)} = \left[\frac{1}{a\times b}\sum_{i=1}^{a}\sum_{j=1}^{b} X_{C(x_i,y_j),p}\right]_{p\times 1} \tag{17}$$

$$\overline{\overline{X}} = \left[\frac{1}{g\times h}\sum_{i=0}^{g-1}\sum_{j=0}^{h-1}\overline{X}_{M(i,j),p}\right]_{p\times 1} \tag{18}$$

$$S^2_{M(x,y),p} = \frac{1}{a\times b-1}\sum_{i=1}^{a}\sum_{j=1}^{b}\left(X_{C(x_i,y_j),p}-\overline{X}_{M(x,y),p}\right)^2 \tag{19}$$

$$S_{M(x,y),p,q} = \frac{1}{a\times b-1}\sum_{i=1}^{a} \times\sum_{j=1}^{b}\left(X_{C(x_i,y_j),p}-\overline{X}_{M(x,y),p}\right)\left(X_{C(x_i,y_j),q}-\overline{X}_{M(x,y),q}\right) \tag{20}$$

$$S^2_p = \frac{1}{g\times h}\sum_{i=0}^{g-1}\sum_{j=0}^{h-1} S^2_{M(i,j),p} \tag{21}$$

$$S_{p,q} = \frac{1}{g\times h}\sum_{i=0}^{g-1}\sum_{j=0}^{h-1} S_{M(i,j),p,q} \tag{22}$$

where $\begin{cases} a = \dfrac{\text{Column size of a multivariate processing unit}}{\text{Column size of a wavelet processing unit}} \\ b = \dfrac{\text{Row size of a multivariate processing unit}}{\text{Row size of a wavelet processing unit}} \end{cases}$, $\begin{cases} g = \dfrac{\text{Column size of an image}}{\text{Column size of a multivariate processing unit}} \\ h = \dfrac{\text{Row size of an image}}{\text{Row size of a multivariate processing unit}} \end{cases}$ and $X_{C(x_a,y_b),p}$ is the pth image characteristic of a wavelet processing unit $C(x_a,y_b)$; $\overline{X}_{M(x,y)}$ is the mean matrix of image characteristics in a multivariate processing unit $M(x,y)$; $\overline{X}_{M(i,j),p}$ is the mean value of the pth image characteristic of $M(i,j)$; $S^2_{M(x,y),p}$ is the variance of the pth image characteristic of $M(x,y)$; $S_{M(x,\ y),\ p,\ q}$ is the covariance of the pth and the qth image characteristics of $M(x,y)$. The multivariate matrices used in this research can be expressed as follows:

$$X_{C(x_a,y_b)} = \begin{bmatrix} A_R(x_a,y_b)\\ D_R(x_a,y_b)\\ A_G(x_a,y_b)\\ D_G(x_a,y_b)\\ A_B(x_a,y_b)\\ D_B(x_a,y_b)\end{bmatrix}_{6\times 1}, \quad \overline{X}_{M(x,y)} = \begin{bmatrix} \overline{A}_R(x,y)\\ \overline{D}_R(x,y)\\ \overline{A}_G(x,y)\\ \overline{D}_G(x,y)\\ \overline{A}_B(x,y)\\ \overline{D}_B(x,y)\end{bmatrix}_{6\times 1} = \begin{bmatrix} \frac{1}{a\times b}\sum_{i=1}^{a}\sum_{j=1}^{b} A_R(x_i,y_j)\\ \frac{1}{a\times b}\sum_{i=1}^{a}\sum_{j=1}^{b} D_R(x_i,y_j)\\ \frac{1}{a\times b}\sum_{i=1}^{a}\sum_{j=1}^{b} A_G(x_i,y_j)\\ \frac{1}{a\times b}\sum_{i=1}^{a}\sum_{j=1}^{b} D_G(x_i,y_j)\\ \frac{1}{a\times b}\sum_{i=1}^{a}\sum_{j=1}^{b} A_B(x_i,y_j)\\ \frac{1}{a\times b}\sum_{i=1}^{a}\sum_{j=1}^{b} D_B(x_i,y_j)\end{bmatrix}_{6\times 1} \tag{23}$$

Normal texture images can be used to estimate the parameters of standard texture characteristics. The sample mean matrix $(\overline{\overline{X}})$ and the sample covariance matrix (S) describe

the properties of and the relations between the image characteristics of normal and defect images. The $\overline{\overline{X}}$ and S are defined below:

$$\overline{\overline{X}} = \begin{bmatrix} \overline{\overline{A}}_R \\ \overline{\overline{D}}_R \\ \overline{\overline{A}}_G \\ \overline{\overline{D}}_G \\ \overline{\overline{A}}_B \\ \overline{\overline{D}}_B \end{bmatrix}_{6\times 1} \tag{24}$$

$\overline{\overline{A}}_R$: Mean value of the approximated characteristic of R component
$\overline{\overline{D}}_R$: Mean value of the synthetic detail characteristic of R component
$\overline{\overline{A}}_G$: Mean value of the approximated characteristic of G component
$\overline{\overline{D}}_G$: Mean value of the synthetic detail characteristic of G component
$\overline{\overline{A}}_B$: Mean value of the approximated characteristic of B component
$\overline{\overline{D}}_B$: Mean value of the synthetic detail characteristic of B component

$$S = \begin{bmatrix} S^2_{A_R} & S_{A_R,D_R} & S_{A_R,A_G} & S_{A_R,D_G} & S_{A_R,A_B} & S_{A_R,D_B} \\ S_{D_R,A_R} & S^2_{D_R} & S_{D_R,A_G} & S_{D_R,D_G} & S_{D_R,A_B} & S_{D_R,D_B} \\ S_{A_G,A_R} & S_{A_G,D_R} & S^2_{A_G} & S_{A_G,D_G} & S_{A_G,A_B} & S_{A_G,D_B} \\ S_{D_G,A_R} & S_{D_G,D_R} & S_{D_G,A_G} & S^2_{D_G} & S_{D_G,A_B} & S_{D_G,D_B} \\ S_{A_B,A_R} & S_{A_B,D_R} & S_{A_B,A_G} & S_{A_B,D_G} & S^2_{A_B} & S_{A_B,D_B} \\ S_{D_B,A_R} & S_{D_B,D_R} & S_{D_B,A_G} & S_{D_B,D_G} & S_{D_B,A_B} & S^2_{D_B} \end{bmatrix}_{6\times 6} \tag{25}$$

where

S^2_p: is the sample variance of the p wavelet characteristic of an image;
$S_{p,q}$: is the sample covariance of the p and q wavelet characteristics of an image.

The T^2 statistic of the multivariate processing unit $M(x,y)$ of a testing image in the multivariate statistical model can be defined as:

$$T^2_{M(x,y)} = a \times b \left[\overline{X}_{M(x,y)} - \overline{\overline{X}}\right]' S^{-1} \left[\overline{X}_{M(x,y)} - \overline{\overline{X}}\right] \tag{26}$$

where

$a \times b$: number of wavelet process units in a multivariate processing unit;
$\overline{X}_{M(x,y)}$: the mean matrix of image characteristics in the multivariate processing unit of a testing image;
$\overline{\overline{X}}$: the mean matrix of image characteristics of a normal image;
S: the covariance matrix of image characteristics of a normal image.

After conducting many experiments, we find 4×4 pixels to be the best size for a multivariate processing unit of the multivariate statistical model when taking into account the following factors: sample training time, recognition time of the testing period, size of the defect area, and other factors in the multivariate processing. Therefore, if a multivariate processing unit $M(x,y)$ of a testing image $g(x,y)$ has a higher T^2 value, it implies that the region contains defects in the testing image. On the contrary, a lower T^2 value signifies that no defect exist in the corresponding region of the image.

In a multivariate control chart, when a T^2 value exceeds the UCL, the process that is operating in the presence of assignable causes is said to be out of control. The presence of assignable causes may result in significant variability in the output of a process and present an unacceptable level of process performance. From the viewpoint of detecting defect image, if the T^2 value of a $M(x,y)$ exceeds the control limit, then the texture properties of the region significantly deviate from those of a normal texture region and can be judged as a defect region. Since the appearances of ripple defects are semi-opaque and fuzzy, the properties of ripple defects are similar to those of a process with small shift from the viewpoint of process control. Thus, this research utilizes wavelet transform to extract valuable features for differentiating ripple defects from normal regions and applies the multivariate statistical model to integrate multiple features and locate the positions of ripple defects in the surfaces of SBL chips.

4. Experiments and analysis

To verify the feasibility of the proposed approach, real SBL images are acquired on a color CCD camera in a laboratory environment. Each colored RGB image has 256×256 pixels in size, three color bands per pixel, and 8 bits of intensity per color band. The database consists of 160 SBL images, of which 31 have no defects and 129 have various ripple defects. All experiments are implemented on a Pentium IV personal computer with 2.44 GHz CPU and 256 MB RAM; and all programming is done in the C language. To demonstrate the feature discrimination of the wavelet characteristics for ripple defects, we study the overlap rates between the defect and the normal regions by using different multivariate statistics in the spatial and the wavelet domains. To evaluate the performance of the proposed wavelet-based multivariate statistical models, we compare defect detection results of applying different multivariate statistics and analyze their ROC curves. Moreover, we also demonstrate the detection effects of the proposed approach under different illumination con-

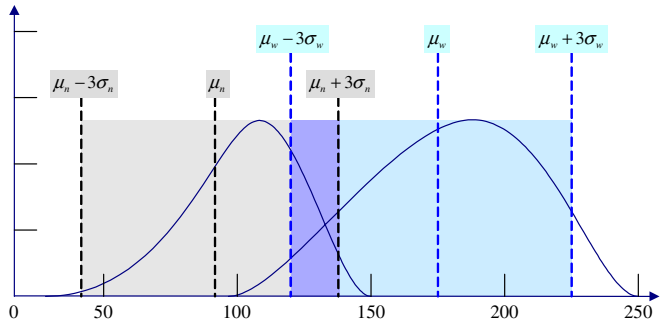

Fig. 4. Overlap between the distributions of defect and normal texture properties.

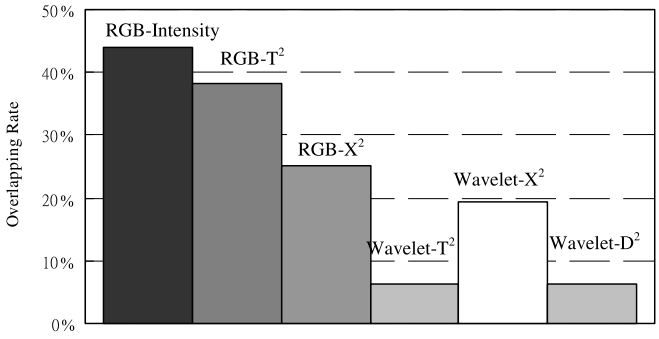

Fig. 5. Overlap rates between the distributions of the defect and the normal texture under different statistical models.

ditions, for ripple defects of various severity levels, and for defects in different texture surfaces.

4.1. Overlap rate comparison of different methods

As shown in Fig. 4, the distribution of the defect texture property may overlap with that of the normal texture property. Let us assume that the texture property of a ripple defect in terms of multivariate statistic (T^2, X^2, or D^2 distance value) is distributed with mean μ_w and variance σ_w^2, and that of a normal texture is distributed with mean μ_n and variance σ_n^2. According to Chebyshev's inequality theorem [42], any random variable X, regardless of its distribution, has a probability of at least $(1 - 1/k^2)$ that X will assume a value within k standard deviations of the mean. Thus, the population mean of any distribution falls between $(\mu - 3\sigma)$ and $(\mu + 3\sigma)$ at a minimum confidence level of 89%. Eq. (27) defines the overlap rate between the two distributions in terms of their means and standard deviations. Dividing the overlapped area by the possible dispersion range of the two distributions, we can obtain the overlap rate, which indicates how fuzzily or easily distinguished the distributions are. When the two distributions are far from each other, they have a small overlap rate and a clear boundary that separates the defect region from the normal region. On the contrary, when the distributions are close to each other, they have a large overlap rate and a fuzzy boundary between the defect and the normal regions. In sum, the larger the overlap rate, the fuzzier the boundary and the more difficult it is to distinguish the defect from the normal texture.

$$
\begin{aligned}
&(1)\ \text{if}\ (\mu_w > \mu_n),\\
&\text{Overlap rate} = \begin{cases} \frac{(\mu_n+3\sigma_n)-(\mu_w-3\sigma_w)}{(\mu_w+3\sigma_w)-(\mu_n-3\sigma_n)} \times 100\% \\ \quad \text{if}\ (\mu_n + 3\sigma_n) - (\mu_w - 3\sigma_w) > 0, \\ 0 \quad \text{otherwise} \end{cases}\\
&(2)\ \text{if}\ (\mu_w < \mu_n),\\
&\text{Overlap rate} = \begin{cases} \frac{(\mu_w+3\sigma_w)-(\mu_n-3\sigma_n)}{(\mu_n+3\sigma_n)-(\mu_w-3\sigma_w)} \times 100\% \\ \quad \text{if}\ (\mu_w + 3\sigma_w) - (\mu_n - 3\sigma_n) > 0. \\ 0 \quad \text{otherwise} \end{cases}
\end{aligned} \tag{27}
$$

Fig. 5 shows the overlap rates between the distributions of the defect and the normal texture under different methods. The proposed wavelet-based multivariate statistical models have lower overlap rates than do those methods that are directly applied to the RGB images. The highest overlap rate in Fig. 5 belongs to the intensity method that integrates RGB components by using 0.299R+0.587G+0.114B, implying that ripple defects are more difficult to be correctly detected from gray level images because of the higher overlap rates. In general, the multivariate statistical methods applied to wavelet domain images are superior to those methods directly applied to raw colored images. Our experimental results demonstrate that the wavelet-based multivariate statistical approach effectively separates the ripple defects from the normal regions.

4.2. Detection results of wavelet-based multivariate statistical models

In the proposed maultivariate statistical models, if X_i does not follow a multivariate normal distribution, we cannot use the pre-defined threshold values (e.g. UCL) to determine whether a transformed value of the statistic (T^2, D^2, or X^2) is large enough for an out-of-control signal. For defect detection, multiple measures of the image features are represented by multiple random variables. Typically, we do not know a priori what distribution each random variable follows, and thereby we use probability plotting to determine whether sample data conform to normal distributions [43]. After the experiments are conducted, the normal probability plots of the six wavelet characteristics constructed from the distributions X_1–X_6 all approximate straight lines, indicating that the multivariate data are normally distributed.

Fig. 6 demonstrates the detection results and the multivariate statistical distance diagrams of the three testing images in Fig. 1 by the Otsu method [44] and the three proposed wavelet-based multivariate statistical methods whose thresholds are described in Sections 2.1–2.3. Apparently, the proposed multivariate statistical models perform better than the Otsu method applied in the spatial domain. The multivariate statistical distance diagrams present the plots

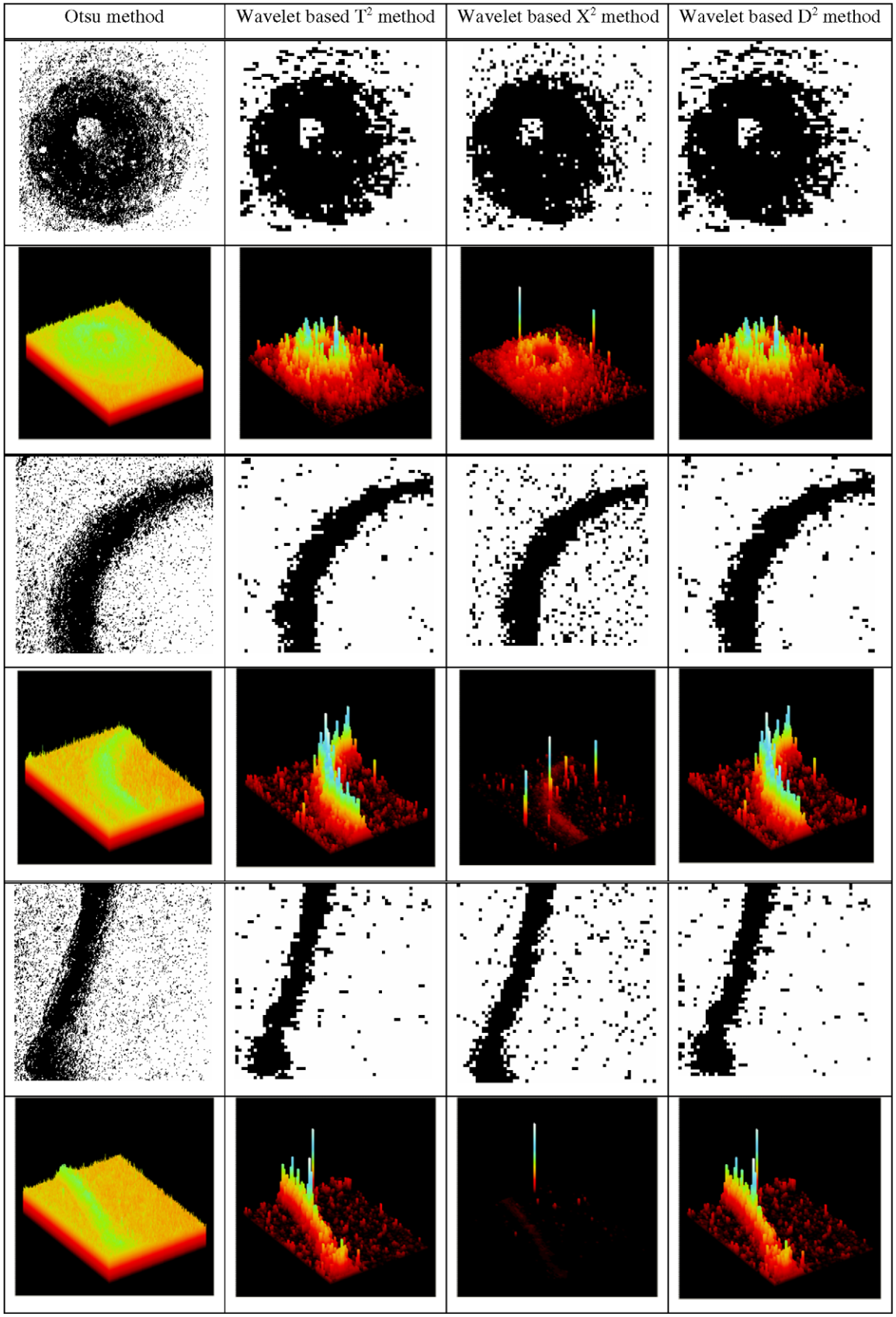

Fig. 6. Detection results and the corresponding distance diagrams of the three testing images in Fig. 1 by Otsu method and the proposed wavelet-based multivariate statistical methods.

of the multivariate statistic values in 3-D perspective, with the peaks indicating the locations of the ripple defects. The detection results are presented as binary images, where pixels with statistic values above the control limit (threshold) are black, and the ones below the control limit are white. It shows that the ripple defects in the original image are detected in the correct locations in the resulting binary image. Noisy points with statistic values above the thresholds may be generated, as seen in Fig. 6. The noisy points in the resulting binary images become small and are scattered throughout the images, whereas the true defects are clustered into large areas. Simple post-processing such as blob analysis can be performed to prevent false alarms.

To verify the performance of the proposed methods, we compare the results of our experiments against those provided by professional inspectors. We evaluate the performance of the three multivariate statistical methods by three objective indices: correct judgment (CR) and erroneous judgments (α and β). CR, the classification rate, is defined as:

$$\mathrm{CR} = 100\% \times (N_{\mathrm{cc}} + N_{\mathrm{dd}})/N_{\mathrm{total}} \tag{28}$$

where N_{cc} is the pixel number of normal textures detected as normal areas, N_{dd} is the pixel number of ripple defects detected as defective regions, and N_{total} is the total pixel number of a testing image. Statistical type I error α suggests the probability of producing false alarms, i.e. detecting normal regions as defects. Statistical type II error β implies the probability of producing missing alarms, which fail to alarm real defects. We divide the area of normal texture detected as defects by the area of actual normal texture to obtain type I error, and the area of undetected defects by the area of actual defects to obtain type II error.

Fig. 7 shows the detection results of the wavelet-based T^2 method at different significance levels. Fig. 8 presents the wavelet-based X^2 method with different standard deviations, and Fig. 9 the wavelet-based D^2 method with different η values. To present the three indices CR, α, and β in the same chart and simplify the performance evaluation process, we convert α into $(1-\alpha)$ and β into $(1-\beta)$; thus, the greater the three indices CR, $(1-\alpha)$, and $(1-\beta)$, the more accurate the detection results. The wavelet-based T^2 method performs well in detecting defects (CR = 90%), when the significance level approaches to 0.0025. The wavelet-based X^2 method achieves good detection results (CR = 88%), when the standard deviation coefficient approximates 1.0. The wavelet-based D^2 method obtains a CR of 89%, when the η value is close to 1.0. All of the three wavelet-based multivariate statistical methods achieve satisfactory performance in detecting ripple defects.

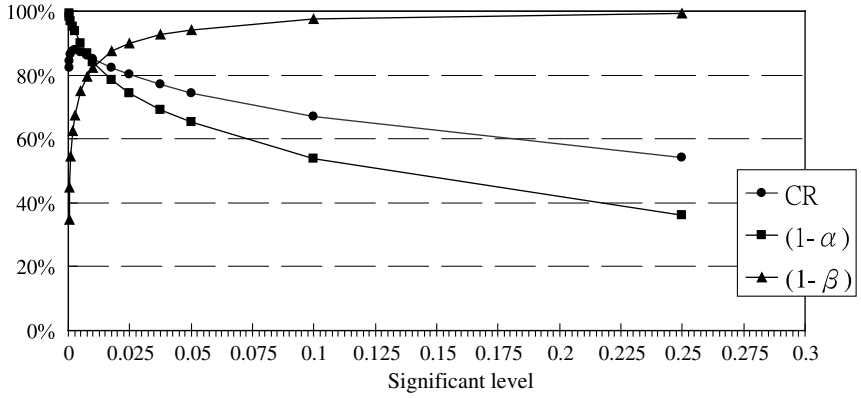

Fig. 7. Detection results of the wavelet-based T^2 method at different significance levels.

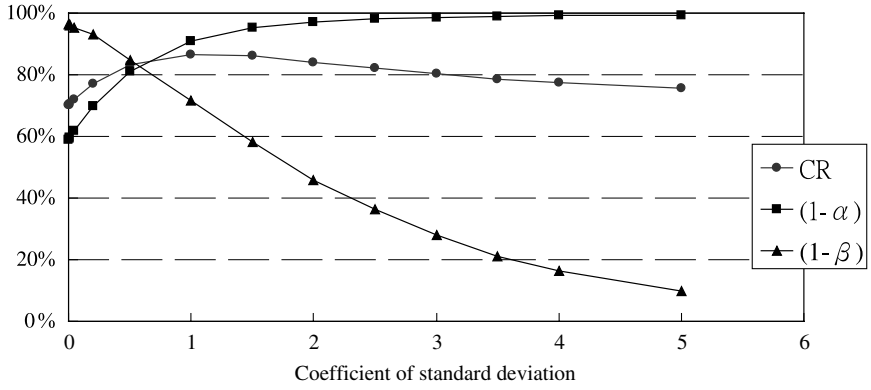

Fig. 8. Detection results of the wavelet-based X^2 method with different standard deviations.

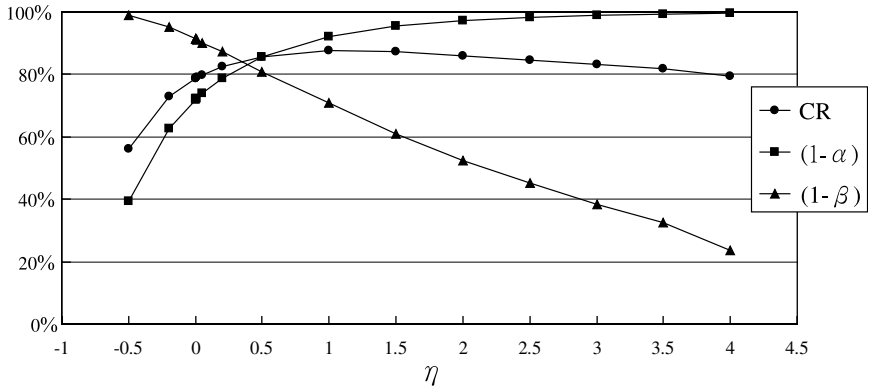

Fig. 9. Detection results of the wavelet-based D^2 method with different η values.

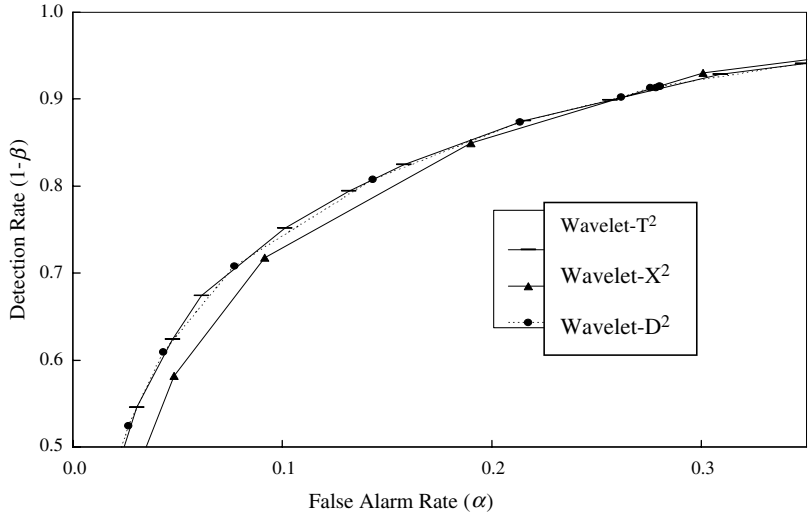

Fig. 10. ROC curves of the wavelet-based T^2, X^2 and D^2 statistical methods.

4.3. ROC curve analyses of three multivariate statistical models

For a given hypothesis testing, different decision thresholds lead to different pairs of false alarm rate (α) and detection rate $(1-\beta)$ that describe the performance of the statistical test. A receiver operating characteristic (ROC) curve plots pairs of the specificity (false alarm rate) and the sensitivity (detection rate) as points when various decision thresholds are used. The plot depicts the tradeoff between the sensitivity and specificity. The ROC curve provides a good standard for comparison of detection methods: for a given false alarm probability, the method providing the highest detection probability can be considered the best. Fig. 10 shows the ROC curves of the wavelet-based T^2, X^2, and D^2 methods by plotting pairs of the false alarm rate and the detection rate of ripple defect detection. The nearer the ROC curve of a test is to the upper-left corner (representing 100 percent detection rate and 0 percent false alarm rate), the better the performance of the test is. Since the ROC curves of the T^2 and the D^2 methods are nearer to the upper-left corner than that of the X^2 method, the T^2 and the D^2 methods perform better than the X^2 method in defect detection with respect to both the false alarm and the detection rate. The ROC curves of the T^2 and the D^2 methods are almost the same. More specifically, the T^2 method is somewhat better than the D^2 method in ripple defect detection.

Fig. 11 compares the three wavelet-based methods at various false alarm rates, when the classification rates (CR), instead of the detection rates $(1-\beta)$, is the subject of interest. All of the three methods can achieve a CR value of more than 85%, when the false alarm rate approaches to 0.05. If we compare the performance at the same false alarm rate, the T^2 and theD^2 methods outperform the X^2 method in overall situation.

Figs. 10 and 11 show that the T^2 and D^2 tests achieve better detection results than does the X^2 test. All of the three tests detect mean shifts, but only the T^2 and the D^2 tests can detect correlation changes among multiple variables. Two reasons can be offered to explain the superior performance of the T^2 and the D^2 tests. First, ripple defects manifest themselves mainly through the mean shifts as well as the correlation changes in the multivariate quality characteristics. Hence, the capability of detecting mean shifts and correlation changes allows the T^2 and the D^2 tests to

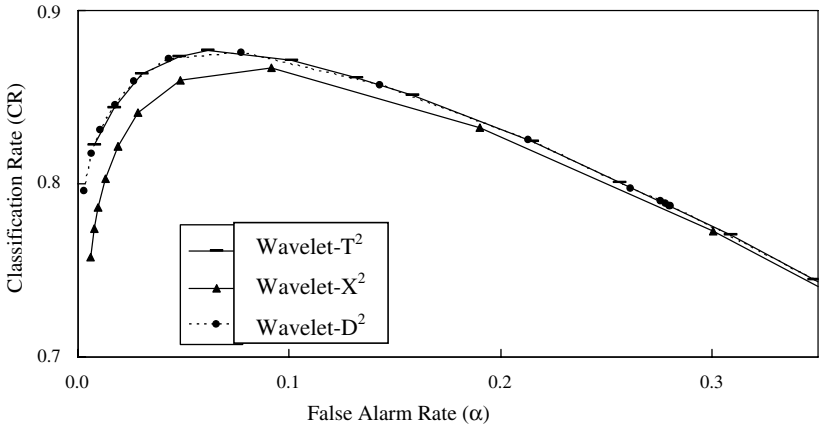

Fig. 11. Curves of classification rates (CR) v.s. false alarm rates (α) of the wavelet-based T^2, X^2 and D^2 methods.

detect ripple defects effectively in the wavelet domain. Second, when detecting relation shifts, the T^2 and the D^2 tests might pick up some normal noises and variations, which lead to correlation changes in the spatial domain. Those correlation changes increase the variance of the T^2 and D^2 test values for normal textures, and thus make the boundary between normal textures and ripple defects less distinctive. The above reasoning is confirmed by the testing results in which the variance of the X^2 test values for normal textures is much less than the variance of the T^2 and the D^2 test values for those defect-free textures in the spatial domain. As to the difference between the T^2 and the D^2 tests, both of them achieve similar detection results. But, the D^2 test does not consider the influence of sample size on the decision of hypothesis testing and does not provide a consistent formal rule of threshold values as discussed in Section 2.4. Therefore, this research primarily applies the T^2 statistic to the wavelet-based multivariate statistical model to detect ripple defects.

4.4. Detection effects at different illumination levels

Because the computation of T^2 is based on the mean vector and covariance matrix of the training samples, experiments are conducted to explore the detection effects at various illumination levels. Underexposed and overexposed versions of the testing images are inspected. Since the intensity levels of ripple defects are darker than those of normal textures, the underexposed versions obtain better detection rates and worse false alarm rates than do the original testing images. On the other hand, the overexposed versions have better false alarm rates and worse detection rates. The results show that the proposed method is moderately sensitive to minor changes (less than 1.5σ of average illumination) in the uniform illumination. But if the illumination changes are significant (more than 3σ of average illumination), the detection effects are degraded. The underexposed (-1.5σ and -3σ) and overexposed ($+1.5\sigma$ and $+3\sigma$) versions of the ripple defect in Fig. 1c are demonstrated in Fig. 12 for visualizing the effect of illumination changes. Fig. 13 shows the ROC curves of various illumination levels. It is recommended to re-compute the mean vector and covariance of the training samples when the illumination of the experimental environment is changed. The training process is quick and easy once the training samples have been selected.

4.5. Detection effects of ripple defects of different severity levels

The multivariate processing procedure of the proposed wavelet-based model converts an image in the spatial domain into a multivariate distance diagram in the frequency domain. The multivariate processing procedure effectively identifies the existence of defects and their precise locations. As this research investigates ripple defects of gradually changing intensity levels, it is important to classify the defects according to their levels of severity. We thus propose the Double-mode thresholding method that classifies defects into two levels (e.g. moderate and serious defects) and the Triple-mode thresholding technique that classifies defects into three levels (e.g. minor, moderate, and serious defects).

Traditional double thresholding methods select two suitable thresholds (T_1 and T_2) as the initial values for segmenting an image into three groups: G_1, G_2 and G_3. G_1 denotes the defect region, G_3 the normal region, and G_2 the region with levels between T_1 and T_2. The G_2 is called the blurred region because it is difficult to judge whether G_2 belongs to the defect or the normal region. To correctly classify G_2, researchers must consider adding other meaningful image properties that can be used as the criterion to judge G_2 pixels. One common judgment criterion is to make use of the image property information of neighboring pixels. The traditional double thresholding algorithm [45] checks each G_2 pixel and reassigns it to G_1 if the pixel has a neighbor in region G_1. The reassigning procedure is repeated until no pixels are reassigned. Then, any pixles left in region G_2 are reassigned to G_3.

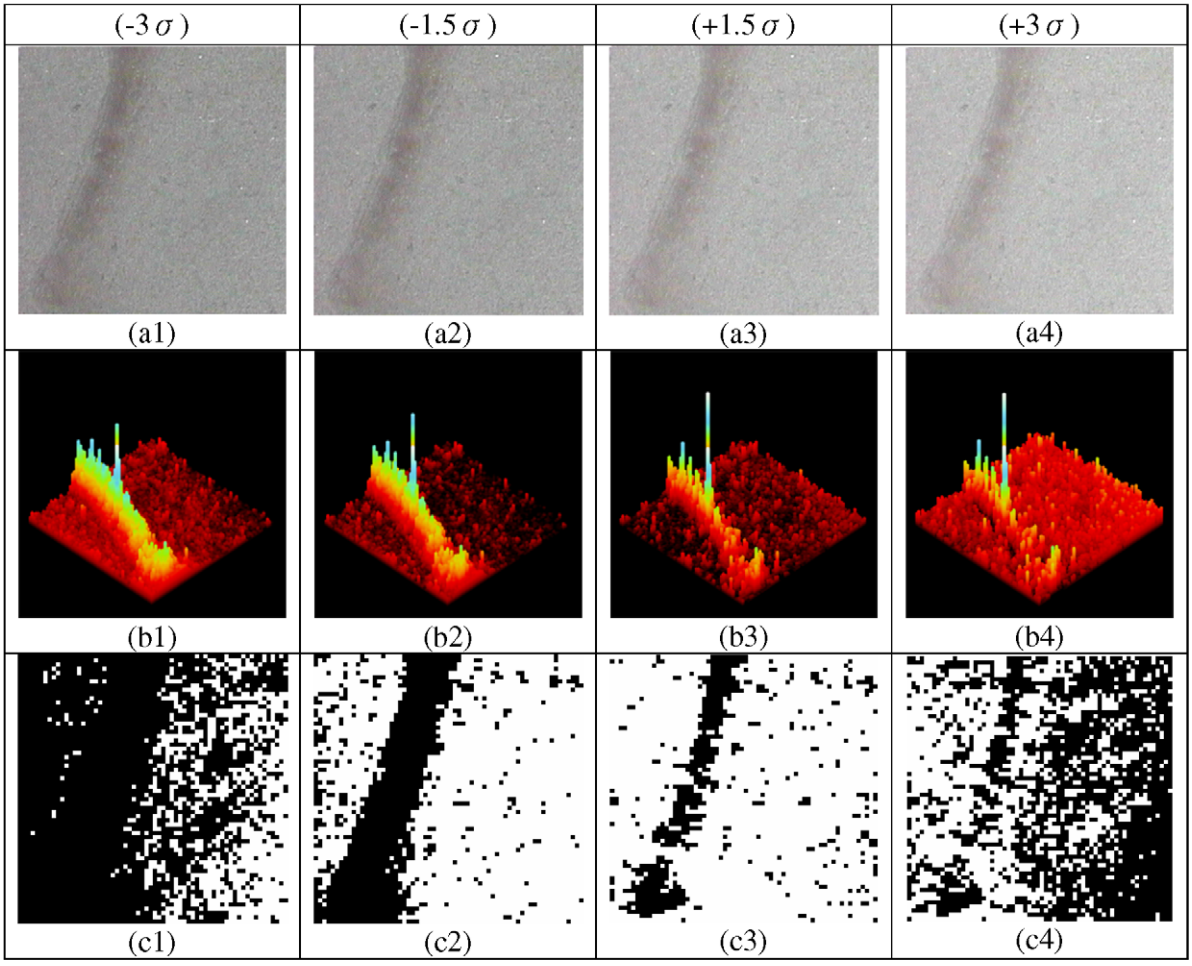

Fig. 12. The effect of changing illumination intensities on Fig. 1(c): (a1)–(a4) the ripple defect surface under underexposed (-1.5σ and -3σ) and overexposed ($+1.5\sigma$ and $+3\sigma$) lighting conditions; (b1)–(b4) the corresponding distance diagrams; (c1)–(c4) the resulting binary images.

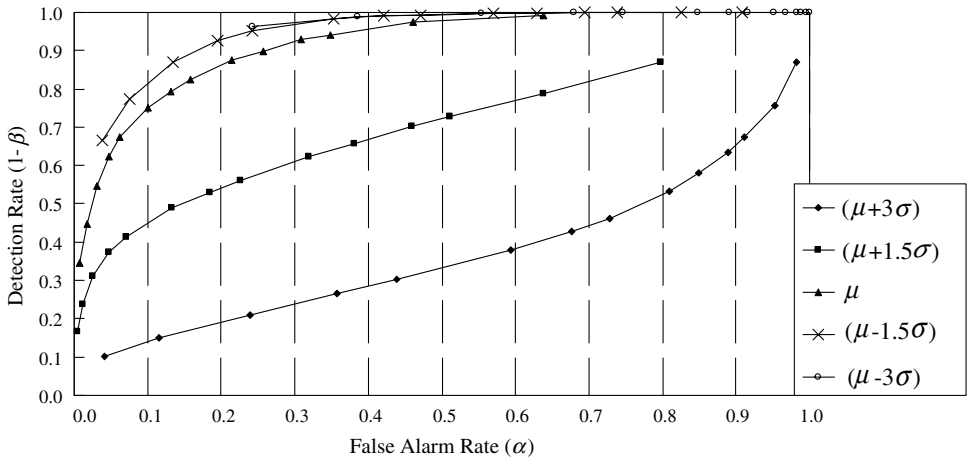

Fig. 13. Detection effects of the proposed method at different illumination levels.

The traditional double thresholding method has a major drawback. Once pixels are assigned to G_1 or G_3, no other criterion can be used to judge whether G_1 or G_3 pixels are correctly classified. Hence, if we apply the traditional double thresholding method to detect defects with gradual intensity level changes, we are very likely to misclassify G_1 or G_3 pixels because of the special image properties of ripple defects. To prevent the misclassification problems, this research improves the traditional double thresholding method and develops the so-called Double-mode and

Triple-mode thresholding methods that take advantage of the statistical mode concept to segment defects with gradual intensity level changes.

The Double-mode thresholding method first performs an Iterative thresholding procedure [45] to determine two initial thresholds (T_1 and T_2) in T^2 domain that segment a testing image into three groups. Then, the Double-mode rules in Eq. (29) are applied to the pixels of the three groups. Supposing a double window has a size of $M \times M$ ($M = 2k + 1$, k is an integer and $1 \leqslant k \leqslant 4$) pixels and the centre of the double window is $(0,0)$, then $C_1(x,y)$ represents the pixel number of the double window of G_1 group. $C_2(x,y)$ and $C_3(x,y)$ denote the pixel numbers of the G_2 and G_3 double windows, respectively. The judgment criteria of the Double-mode rules can be expressed as follows:

$$\begin{aligned}
&\text{if } [C_1(x,y) > C_2(x,y) \quad \& \quad C_1(x,y) > C_3(x,y)] \\
&\quad f(x,y) \in G_1 \\
&\text{else if } [C_2(x,y) > C_1(x,y) \quad \& \quad C_2(x,y) > C_3(x,y)] \\
&\quad f(x,y) \in G_2 \\
&\text{else if } [C_3(x,y) > C_2(x,y) \quad \& \quad C_3(x,y) > C_1(x,y)] \\
&\quad f(x,y) \in G_3 \\
&\text{else} \\
&\quad f(x,y) \in G_i(x,y)
\end{aligned} \tag{29}$$

where $G_i(x,y)$ is the original group at (x,y).

The procedures of the Triple-mode thresholding are similar to those of the Double-mode method except that the former has one more group number than the latter. Furthermore, the window sizes of the Double-mode and the Triple-mode thresholdings are both set at 7×7 pixels because this specific size surpasses other sizes in detection of defects according to the results of our experiments.

Fig. 14 shows six different ripple defects, the first three of which are processed by the wavelet-based multivariate T^2 model and the Double-mode thresholding; and the rest of which are processed by the same statistical model and the Triple-mode thresholding. The detection results of the Double-mode thresholding are presented in Fig. 14(a), in which the defect regions are divided into two types: moderate defects (denoted as intensity = 155) and serious defects (intensity = 0). The detection results of the Triple-mode thresholding are shown in Fig. 14(b), in which the defect regions are divided into three types: minor defects (intensity = 200), moderate defects (intensity = 100) and serious defects (intensity = 0). The ripple defects are not only detected but also classified based on their degrees of deviation from the normal texture property. The proposed wavelet-based multivariate T^2 statistical model achieves a 93.75% accuracy rate of detection; that is, 150 of the total 160 SBL images are correctly detected as with or without ripple defects. Two of the 31 faultless images are detected as defective (a 6.4% false alarm rate), and 8 of the 129 images that contain ripple defects are not detected as defective (a 6.2% missing alarm rate).

4.6. Detection results of defects in different texture surfaces

The proposed wavelet-based multivariate T^2 statistical method detects not only the ripple defects but also other kinds of surface defects. To evaluate its performance in detecting common surface defects, we apply the developed statistical model to the surface defect images that have been used in literature [9,10,16]. Because the common defect images in the above literature are in gray scale (not in colour as the ripple defect images of this research), the number of image characteristics is reduced from six to two. And, the UCL of the T^2 control chart according to Eq. (8) is used as as the decision criterion for defect detection in this section. Fig. 15 presents the partial detection results of common defect images that are used in the above literature. Defects in three different texture surfaces (grid, directional, and random textures) are detected by the proposed method. All of the defects are correctly identified and some very small normal regions are detected as defects.

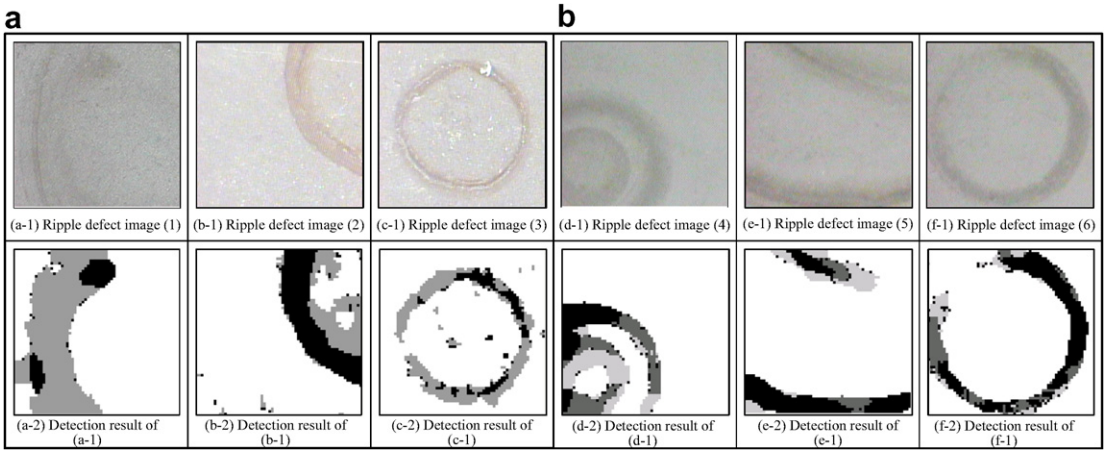

Fig. 14. Six ripple defect images and their detection results of the wavelet-based multivariate T^2 statistical model followed by Double-mode or Triple-mode thresholding.

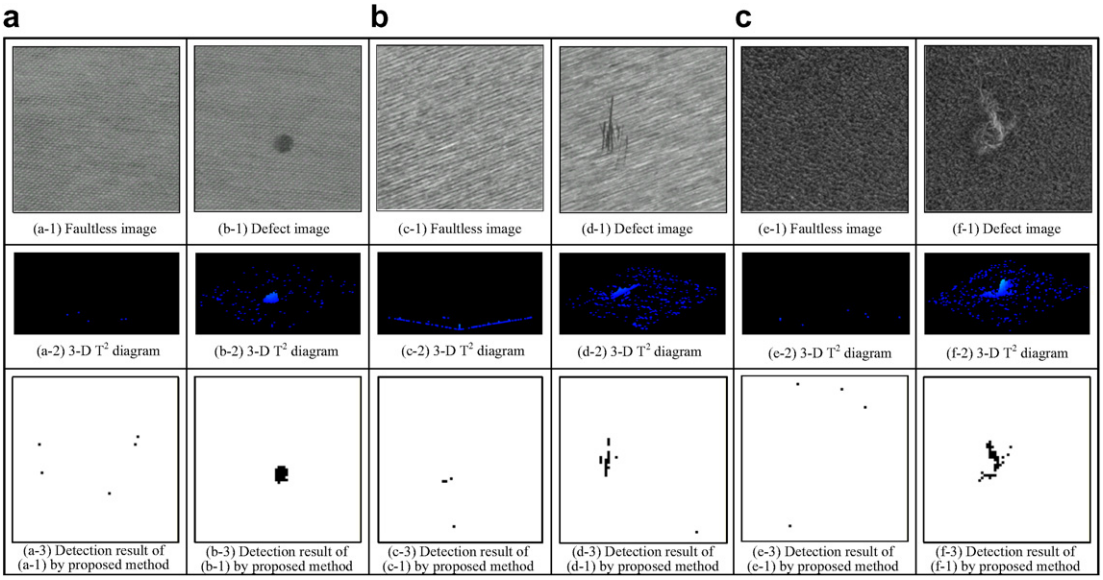

Fig. 15. Defects in different texture surfaces and their detection results by the the wavelet-based T^2 statistical method.

The proposed model, like the detection methods described in the literature review, achieves good performance in detection of common surface defects. But, besides of detecting fuzzy surface defects with gradually changing intensity levels, the wavelet-based multivariate approach possesses some properties that the other methods do not have. Advantages of the proposed model are summarized as follows:

1. The proposed method can accurately identify the locations of the defects; only very small deviations exist between the detected defect locations and the real defect regions. The maximum possible deviation is only 4 pixels because one wavelet processing unit has a size of 2×2 pixels and one multivariate processing unit contains 2×2 wavelet processing units.
2. The proposed model offers great flexibility for detecting defects of differing complexity. The type and the number of image characteristics in the multivariate processing procedure can be adjusted to suit the needs of various image detection tasks.
3. Since the proposed wavelet-based multivariate statistical approach applies local image processing, processing time is greatly saved. For instance, it takes 2 s to process a colour image of 256×256 pixels. Also, in the training stage, it takes less than 1 s to calculate related multivariate parameters when a suitable image is selected in advance.

5. Conclusions

In this paper, we have presented a wavelet-based multivariate statistical approach for detecting ripple defects in colored texture surfaces. The proposed method can not only detect any unanticipated ripple defects as long as they break the homogeneity of textures but also classify the types of defects according to their levels of severity. Three multivariate statistics of Hotelling T^2, Mahalanobis distance D^2, and Chi-square X^2, are investigated to integrate the multiple texture features and judge the existence of ripple defects.

Capable of capturing the correlation structures of multiple variables and detecting relation shifts and mean shifts, the T^2 and the D^2 tests are superior in detecting ripple defects than the X^2 test which detects only mean shifts. Because ripple defects may manifest not only through mean shifts but also through correlation changes, we can improve the accuracy of defect detection by suppressing noises and variations in normal textures, which cause correlation changes. It appears that a more rigorous multivariate analysis technique detecting mean shifts and correlation changes is necessary for ripple defect detection.

The proposed method is based on feature extraction from wavelet-domain images for defect detection. Since the computation of multivariate statistic is based on the mean vector and covariance matrix of training samples, the lighting changes may lead to the increase of variation in statistics and result in affecting the effect of defect detection. It is recommended to re-compute the mean vector and covariance of the training samples when illumination is significantly changed. Future research may extend the proposed method to similar lowcontrast defect detection problems, such as abnormal inspection of medical images and oxidization defect detections of leadframes.

Acknowledgement

The author thanks the National Science Council of Taiwan (ROC) for the financial support through the Grant NSC 90-2212-E-324-004.

References

[1] M.H. Bharati, J. Jay Liu, F. MacGregor, Image texture analysis: methods and comparisons, Chemometrics and Intelligent Laboratory Systems 72 (2004) 57–71.

[2] A. Pikaz, A. Averbuch, An efficient topological characterization of gray-levels textures using a multiresolution respresentation, Graphical Models and Image Processing 59 (1997) 1–17.

[3] A. Kumar, Neural network based detection of local textile defects, Pattern Recognition 36 (2003) 1645–1659.

[4] A. Abouelela, H.M. Abbas, H. Eldeeb, A.A. Wahdan, S.M. Nassar, Automated vision system for localizing structural defects in textile fabrics, Pattern Recognition Letters 26 (2005) 1435–1443.

[5] D. Chetverikov, A. Hanbury, Finding defects in texture using regularity and local orientation, Pattern Recognition 35 (2002) 2165–2180.

[6] T. Fang, M.A. Jafari, S.C. Danforth, A. Safari, Signature analysis and defect detection in layered manufacturing of ceramic sensors and actuators, Machine Vision and Applications 15 (2003) 63–75.

[7] T. Kubota, P. Talekar, X. Ma, T.S. Sudarshan, A nondestructive automated defect detection system for silicon carbide wafers, Machine Vision and Applications 16 (2005) 170–176.

[8] M.H. Ahmed Fadzil, C.J. Weng, LED cosmetic flaw vision inspection system, Pattern Analysis and Applications 1 (1998) 62–70.

[9] D.M. Tsai, S.K. Wu, Automated surface inspection using Gabor filters, International Journal of Advanced Manufacturing Technology 16 (2000) 474–482.

[10] D.M. Tsai, S.K. Wu, M.C. Chen, Optimal Gabor filter design for texture segmentation using stochastic optimization, Image and Vision Computing 19 (2001) 299–316.

[11] L.H. Siew, R.M. Hodgson, E.J. Wood, Texture measures for carpet wear assessment, IEEE Transactions on Pattern Analysis and Machine Intelligence 10 (1988) 92–105.

[12] K. Venkat Ramana, B. Ramamoorthy, Statistical methods to compare the texture features of machined surfaces, Pattern Recognition 29 (1996) 1447–1459.

[13] C.H. Chan, K.H. Pang, Fabric defect detection by Fourier analysis, IEEE Transactions on Industry Application 36 (2000) 1267–1276.

[14] D.M. Tsai, C.H. Chiang, Automated band selection for wavelet reconstruction in the application of defect detection, Image and Vision Computing 21 (2003) 413–431.

[15] Ajay Kumar, K.H. Pang, Defect detection in textured materials using Gabor filters, IEEE Transactions on Industry Applications 38 (2002) 425–440.

[16] D.M. Tsai, B. Hsiao, Automatic surface inspection using wavelet reconstruction, Pattern Recognition 34-6 (2001) 1285–1305.

[17] S.G. Mallat, A theroy for mulitiresolution signal decomposition the wavelet representation, IEEE Transactions on Pattern Analysis and Machine Intelligence 11–7 (1989) 674–693.

[18] M. Tico, P. Kuosmanen, J. Saarinen, Wavelet domain features for fingerprint recognition, Electronics Letters 37–1 (2001) 21–22.

[19] M.N. Shirazi, H. Noda, N. Takao, Texture classification based on Markov modeling in wavelet feature space, Image and Vision Computing 18 (2000) 967–973.

[20] S. Arivazhagan, L. Ganesan, Texture segmentation using wavelet transform, Pattern Recognition Letters 24 (2003) 3197–3203.

[21] C. Garcia, G. Zikos, G. Tziritas, Wavelet packet analysis for face recognition, Image and Vision Computing 18-4 (2000) 289–297.

[22] A. Latif-Amet, A. Ertuzun, A. Ercil, An efficient method for texture defect detection: sub-band domain co-occurrence matrices, Computers and Geosciences 28 (2002) 763–774.

[23] K. Huang, S. Aviyente, Information-theoretic wavelet packet sub-band selection for texture classification, Signal Processing 86 (2006) 1410–1420.

[24] Peiling Cui, Junhong Li, Quan Pan, Hongcai Zhang, Rotation and scaling invariant texture classification based on Radon transform and multiscale analysis, Pattern Recognition Letters 27 (2006) 408–413.

[25] P.-H. Suen, G. Healey, Modeling and classifying color textures using random fields in a random environment, Pattern Recognition 32 (1999) 1009–1017.

[26] K.Y. Song, J. Kittler, M. Petrou, Defect detection in random colour textures, Image and Vision Computing 14 (1996) 667–683.

[27] G. Van de Wouwer, P. Scheunders, S. Livens, D. Van Dyck, Wavelet correlation signatures for color texture characterization, Pattern Recognition 32 (1999) 443–451.

[28] H.Y.T. Nagan, G.K.H. Pang, S.P. Yung, M.K. Ng, Wavelet based methods on patterned fabric defect detection, Pattern Recognition 38 (2005) 559–576.

[29] H. Hotelling, Multivariate quality control, in: C. Eisenhart, M.W. Hastay, W.A. Wallis (Eds.), Techniques of Statistical Analysis, McGraw-Hill, New York, NY, 1947, 111–184.

[30] F.B. Alt, Multivariate quality controlEncyclopedia of Statistical Sciences, John Wiley & Sons, New York, NY, 1985, 110-122.

[31] J.K. Jolayemi, A power function model for determining sample size for the operations of multivariate control chart, Computational Statistic & Data Analysis 20 (1995) 633–641.

[32] R.L. Mason, J.C. Young, Improving the sensitivity of the T^2 statistic in multivariate process control, Journal of Quality Technology 31-2 (1999) 155–165.

[33] R.L. Mason, Y.M. Chou, J.C. Young, Applying Hotelling's T^2 statistic to batch processes, Journal of Quality Technology 33-4 (2001) 466–479.

[34] E.B. Martin, A.J. Morris, C. Kiparissides, Manufacturing performance enhancement through multivariate statistical process control, Annual Review in Control 23 (1999) 35–44.

[35] C. Wikstrom, C. Albano, L. Eriksson, H. Friden, E. Johansson, A. Nordahl, S. Rannar, M. Sandberg, N. Kettaneh-Wold, S. Wold, Multivariate process and quality monitoring applied to an electroysis process. Part I- Process supervision with multivariate control chart, Chemometrics and Intelligent Laboratory System 42 (1998) 211–231.

[36] C. Wikstrom, C. Albano, L. Eriksson, H. Friden, E. Johansson, A. Nordahl, S. Rannar, M. Sandberg, N. Kettaneh-Wold, S. Wold, Multivariate process and quality monitoring applied to an electroysis process. Part II- Multivariate time-series analysis of lagged latent variables, Chemometrics and Intelligent Laboratory System 42 (1998) 233–240.

[37] C.A. Lowry, D.C. Montgomery, A review of multivariate control charts, IIE Transactions 27 (1995) 800–810.

[38] D.C. Montgomery, Multi-variate Process Monitoring and Control, Fifth ed.Introduction to Statistical Quality Control, John Wiley & Sons, Hoboken, NJ, 2005, 486–522.

[39] N. Ye, S.M. Emran, Q. Chen, S. Vilbert, Multivariate statistical analysis of audit trails for host-based intrusion detection, IEEE Transactions on Computers 51–7 (2002) 810–820.

[40] T.P. Ryan, Multivariate control charts for measurement data. Statistical Methods for Quality Improvement, second ed., John Wiley & Sons, Inc., NY, 2000, pp. 253–268.

[41] J.F. Hair Jr., Rolph E. Anderson, Ronald L. Tatham, William C. Black, Multivariate Data Analysis, fifth ed., Prentice Hall, Upper Saddle River, NJ, 1998, 223-224.

[42] R.E. Walpole, R.H. Myers, S.L. Myers, Probability and Statistics for Engineering and Scientists, Sixth ed., Prentice Hall, Upper Saddle River, NJ, 1998, 108–109.

[43] Douglas C. Montgomery, George C. Runger, Applied Statistics and Probability for Engineers, second ed., Johj Wiley & Sons, Inc., 1999, 170-173.

[44] N. Otsu, A threshold selection method from gray level histograms, IEEE Transactions on Systems, Man and Cybernetics 9 (1979) 62–66.

[45] J. Ramesh, K. Rangachar, G.S. Brain, Machine Vision. Interational editions, Mcgraw-Hill, New York, NY, 1995, 76–86.